10-2000

Sn/Ge(111) Surface Charge-Density-Wave Phase Transition

T. E. Kidd
University of Illinois at Urbana-Champaign

T. Miller
University of Illinois at Urbana-Champaign

See next page for additional authors

Sn/Ge(111) Surface Charge-Density-Wave Phase Transition

T. E. Kidd,[1] T. Miller,[1] M. Y. Chou,[2] and T.-C. Chiang[1,*]

[1]*Department of Physics, University of Illinois at Urbana-Champaign, 1110 West Green Street, Urbana, Illinois 61801-3080 and Frederick Seitz Materials Research Laboratory, University of Illinois at Urbana-Champaign, 104 South Goodwin Avenue, Urbana, Illinois 61801-2902*

[2]*School of Physics, Georgia Institute of Technology, Atlanta, Georgia 30332-0430*

(Received 4 May 2000)

Angle-resolved photoemission has been utilized to study the surface electronic structure of $\frac{1}{3}$ monolayer of Sn on Ge(111) in both the room-temperature $(\sqrt{3} \times \sqrt{3})R30°$ phase and the low-temperature (3×3) charge-density-wave phase. The results reveal a gap opening around the (3×3) Brillouin zone boundary, suggesting a Peierls-like transition despite the well-documented lack of Fermi nesting. A highly sensitive electronic response to doping by intrinsic surface defects is the cause for this unusual behavior, and a detailed calculation illustrates the origin of the (3×3) symmetry.

PACS numbers: 73.20.At, 68.35.Rh, 71.45.Lr, 79.60.Dp

The recent discovery of a charge-density-wave (CDW) transition in $\frac{1}{3}$-monolayer Sn on Ge(111) [1–4] has stimulated much interest, yet surprisingly no consensus has been reached regarding the nature of the transition. This system represents a prototype for charge-ordered states in reduced dimensions, and an intriguing aspect of the phase transition is the coexistence of phases over a wide temperature range. This inhomogeneous phase mixture is a basic hallmark for a broad class of important "complex functional materials." Examples include the stripe phase in high-temperature superconductors and the chemical and dipolar nanodomains in relaxor ferroelectrics and colossal magnetoresistive materials, which remain poorly understood despite an intense effort on a national scale [5].

The Sn/Ge surface exhibits a $(\sqrt{3} \times \sqrt{3})R30°$ reconstruction at room temperature, ideally with each unit cell containing one Sn atom in the T_4 adsorption site. The threefold bonding for the Sn atom leaves an electron in the dangling bond, giving rise to a half-filled surface band. As the temperature is lowered below ~210 K, the system transforms gradually and becomes a fully developed (3×3) phase below ~100 K. In this low-temperature CDW phase, each unit cell contains three Sn atoms, two positively charged and one negatively charged. Such CDW transitions are usually driven by electron-phonon coupling enhanced by Fermi surface nesting, but calculations have indicated no nesting for Sn/Ge(111) [6,7]. Alternative models that have been put forth include a rehybridization mechanism [8], an order-disorder transition [9], a dynamic fluctuation model [10], and a mechanism involving strong electron correlation [11]. Related to this debate is the question whether the (3×3) surface is metallic, semiconducting, or insulating with a correlation gap.

Results from previous angle-resolved photoemission studies have been confusing. Goldoni and Modesti [11] observed a dispersive peak in the normal phase transforming into a nondispersive peak in the CDW phase accompanied by a depletion of the density of states near the Fermi level. These observations were taken as evidence for strong electron correlation effects. However, this interpretation was later rejected by Uhrberg and Balasubramanian [9], who observed dispersive peaks crossing the Fermi level for both phases. They suggested that the $(\sqrt{3} \times \sqrt{3})R30°$ phase was just a structurally disordered state of the (3×3) phase. A similar model invoking dynamic fluctuation as the source of disorder was proposed by Avila *et al.* [10]. However, these models based on disorder were contradicted by x-ray studies [12]. A key issue neglected in many of the previous studies is that the system inevitably contains defects that are Ge atoms substituting for Sn atoms in the top layer. At a concentration of just ~3%, the defects nonetheless play an important role as revealed by scanning tunneling microscopy (STM) [1–4]. They induce a CDW phase in surrounding areas in an otherwise $(\sqrt{3} \times \sqrt{3})R30°$ surface at room temperature. This mixed phase has been verified by photoemission studies of the Sn core level line shape [13].

In this paper, we present new angle-resolved photoemission measurements of the valence structure of Sn/Ge(111), with a focus on the (3×3) zone boundary. Despite the lack of nesting as noted above, a gap opening is seen all around the (3×3) zone boundary. Taking into account the mixed phase at room temperature, the results yield band dispersions in excellent agreement with theory. The key new concept here is that a slight change in state occupancy due to defect doping leads to large changes in electronic response, resulting in a Peierls-like (3×3) instability. This confirms an earlier suggestion of Melechko *et al.* based on STM studies that the phase transition is defect mediated [1–4].

Our measurements were performed at the Synchrotron Radiation Center in Stoughton, Wisconsin. All spectra shown were taken with a photon energy of 10 eV. Figure 1 shows a comparison between spectra taken at 80 and 300 K at several points in k space. The inset shows the $(\sqrt{3} \times \sqrt{3})R30°$ and (3×3) Brillouin zones as the large and small hexagons, respectively, and the curve represents the $(\sqrt{3} \times \sqrt{3})R30°$ holelike Fermi surface based on a

 0031-9007/00/85(17)/3684(4)$15.00

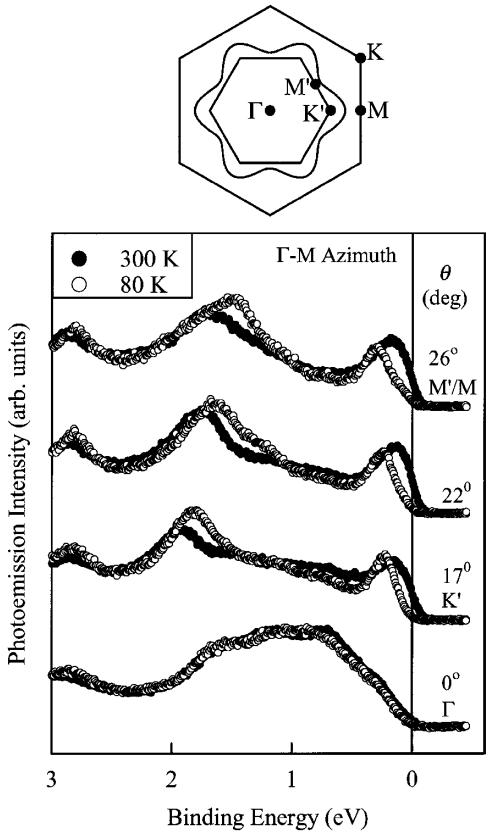

FIG. 1. Comparison of photoemission spectra taken at 80 and 300 K for polar emission angles of 0°, 17°, 22°, and 26° along the Γ-M azimuth. They correspond to Γ, K', midway between K' and M'/M, and M'/M in the Brillouin zone. The inset shows the $(\sqrt{3} \times \sqrt{3})R30°$ Brillouin zone (large hexagon), the (3×3) Brillouin zone (small hexagon), and the $(\sqrt{3} \times \sqrt{3})R30°$ Fermi surface (curve).

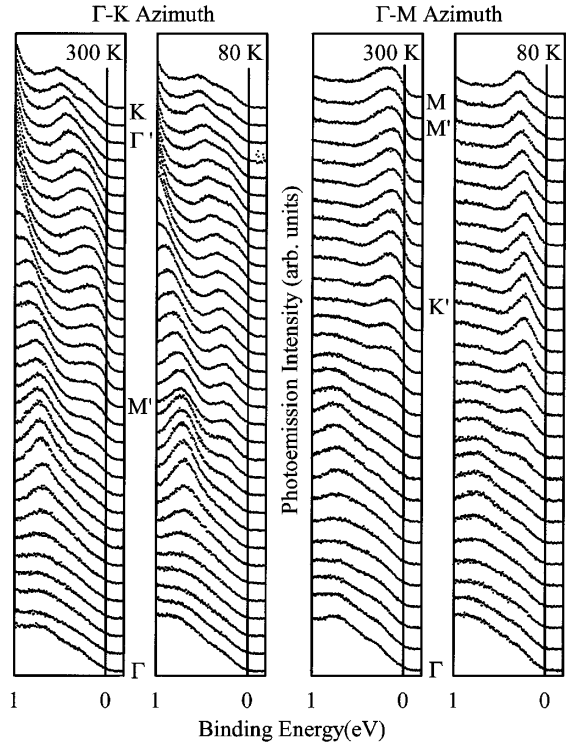

FIG. 2. Photoemission spectra taken at 80 and 300 K along the Γ-K and Γ-M azimuths. In each set, the spectra are taken with a 1° increment in polar angle starting from the bottom spectrum taken at normal emission. For features near the Fermi level, the approximate locations in k space are indicated.

local-density-approximation (LDA) calculation [2,6]. As mentioned above, this Fermi surface and the (3×3) zone do not nest. The bottom spectra in Fig. 1, taken at normal emission (Γ), are nearly identical for the two phases. The other three sets of spectra were taken with polar emission angles 17°, 22°, and 26° along the Γ-M azimuth, and correspond to K', midway between K' and M', and M' on the (3×3) zone boundary, respectively. These are representative of what happens around the (3×3) zone boundary—a well-developed Fermi edge at 300 K is replaced by a gap at 80 K. A careful examination of data taken at various angles (e.g., the bottom spectra in Fig. 1) and at higher binding energies to include the Ge substrate emission features shows that this gap opening is not due to a surface photovoltage effect as previously claimed [9].

A full set of spectra, taken along the Γ-M and Γ-K azimuths at 1° polar angle increments starting from the bottom spectra at normal emission, is shown in Fig. 2. The additional data along Γ-M reinforce our discussion above. The leading peak at 300 K is much wider than that at 80 K, and the line shape suggests that the peak is likely composed of unresolved components. The Γ-K azimuth was emphasized in previous studies [9–11]. The 80 K data show three dispersive peaks. The two near the Fermi level are derived from the Sn dangling bonds, and one of them appears to cross the Fermi level, in agreement with Ref. [9]. About midway between M' and K, the valley between the two peaks at 80 K becomes filled in to form a broad feature at 300 K. A careful analysis shows that this line shape cannot be accounted for by broadening of the 80 K spectra. Rather, the results can be well represented by the addition of a new peak located between the two original peaks. There is a strong rationale for this interpretation. As discussed above, the surface at 300 K is actually a mixture of the $(\sqrt{3} \times \sqrt{3})R30°$ and the (3×3) phases. A single peak is expected for the pure $(\sqrt{3} \times \sqrt{3})R30°$ phase, which should split into two for the (3×3) phase. Thus, a total of three peaks is expected for the mixed phase at 300 K. This complication was the source of confusion in earlier studies.

Figure 3 shows difference spectra along the two azimuths obtained by subtracting the 80 K data from the 300 K data, with each pair of spectra normalized to the same integrated intensity between 0 and 4 eV binding energy. The phase transition causes a transfer of spectral weight among the different peaks. The difference spectra along each direction show a major peak near the Fermi level, as expected, which should correspond to the pure

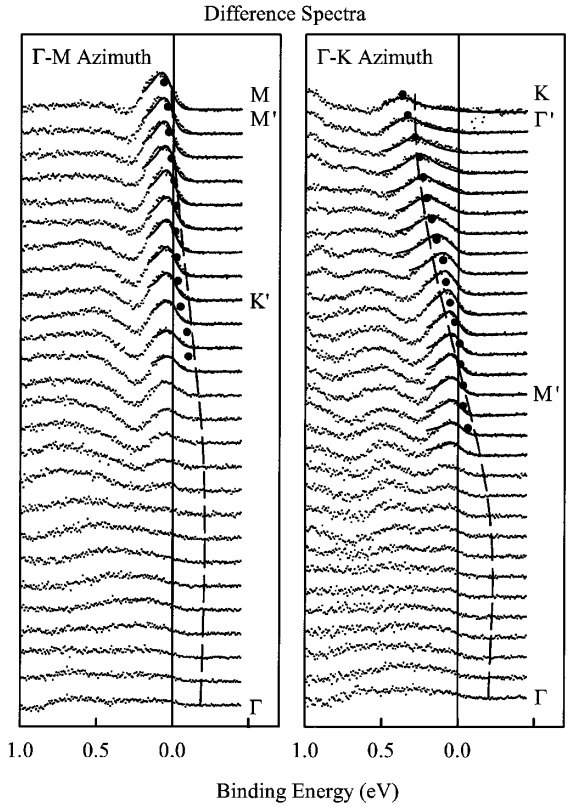

FIG. 3. Difference spectra along the Γ-K and Γ-M azimuths obtained by subtracting the 80 K spectra from the 300 K spectra. The curves through the data points are best fits, and the dashed curves are dispersion curves based on a band structure calculation.

$(\sqrt{3} \times \sqrt{3})R30°$ phase. Some weak negative features are also expected and observed, but these are unimportant for the present discussion. The solid curves through the data points are best fits assuming a Lorentzian peak with constant width multiplied by the Fermi-Dirac function. A constant peak width is compatible with the notion that the width is dominated by defect scattering. While the peak is below the Fermi level, its intensity remains fairly constant from the fit. Thus, it is reasonable to extend the analysis over a limited range as the peak moves above the Fermi level, leaving only a tail in the spectra. The peak positions deduced from the fit are shown as circles in Fig. 3, and the peak intensities vary by less than 10% near and above the Fermi level. The dashed curves indicate the expected peak dispersions for the pure $(\sqrt{3} \times \sqrt{3})R30°$ phase based on a LDA calculation [6]. They are in good agreement with the experiment.

The bottom panel of Fig. 4 illustrates again the good agreement between the calculated LDA band (curve) [6] and our results (circles). As noted above, the Fermi surface does not mesh with the (3×3) zone, yet the 300 K spectra in Fig. 1 indicate a Fermi edge all around the (3×3) zone boundary. This region of "extended Fermi edge" is indicated in the bottom panel of Fig. 4. Note that the band dispersion lies within just several tens of meV within the

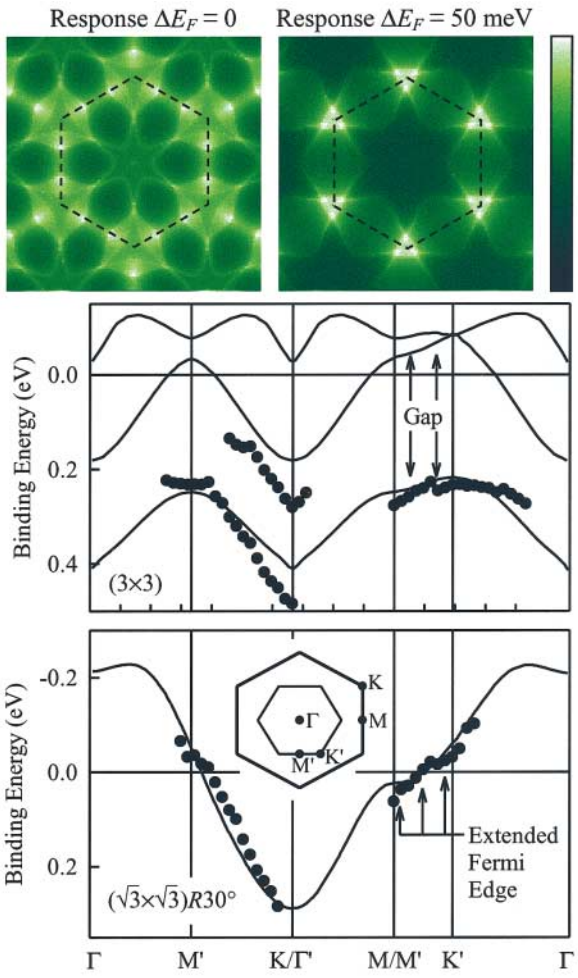

FIG. 4 (color). Theoretical band dispersions (curves) and experimental results (circles) for the (3×3) phase (middle panel) and the $(\sqrt{3} \times \sqrt{3})R30°$ phase (bottom panel). The color maps on top show the calculated Lindhard response functions for the ideal $(\sqrt{3} \times \sqrt{3})R30°$ phase and the same with the Fermi level shifted upward by 50 meV relative to the band. The dashed hexagons indicate the $(\sqrt{3} \times \sqrt{3})R30°$ Brillouin zone. The color bar to the right indicates the conversion between linear intensity and color levels.

Fermi level. The finite peak width and the low dispersion along the K'-M' segment conspire to give rise to the extended Fermi edge. The good match with the (3×3) zone boundary suggests a Peierls-like transition, but the lack of (3×3) Fermi nesting argues strongly against it.

The circles in the middle panel of Fig. 4 show the measured band dispersions for the (3×3) phase. The solid curves are theoretical results from an LDA calculation with electron correlation (on-site Coulomb interaction) included within a generalized Hubbard model [7]. The agreement between experiment and theory is quite good. Between M' and Γ', the single band for the $(\sqrt{3} \times \sqrt{3})R30°$ phase (bottom panel) is split into three bands in the (3×3) phase. The lower two bands are observed by photoemission, and the highest band is unoccupied and therefore not

observed. Between M' and K', the $(\sqrt{3} \times \sqrt{3})R30°$ band also splits into three bands in the (3×3) phase. Only the lowest band is occupied, and its energy is much lower than the corresponding $(\sqrt{3} \times \sqrt{3})R30°$ band near the Fermi level. This energy shift accounts for the apparent gap opening in the spectra around the (3×3) zone boundary.

The same LDA-Hubbard calculation [7] shows that the $(\sqrt{3} \times \sqrt{3})R30°$ and (3×3) phases have nearly the same energy, with a difference of just a few meV per Sn atom. Thus, it is not surprising that seemingly minor perturbations caused by surface defects can induce the phase transition locally at room temperature as observed by STM [1–4]. We now examine the detailed mechanism for this induced transition and the reason for the (3×3) symmetry. The defects, being electron donors based on STM studies [1–4], can cause an upward shift of the local Fermi level. Shown in the top of Fig. 4 are calculated Lindhard response functions $\chi(\mathbf{k})$, presented as two-dimensional color maps, using the band dispersion in [6]. In each map, the hexagonal $(\sqrt{3} \times \sqrt{3})R30°$ Brillouin zone is indicated. The map on the left, labeled $\Delta E_F = 0$ (unshifted Fermi level), shows no particular features at the hexagon corners (K), in agreement with earlier calculations indicating poor nesting [6]. The map on the right is for a small upward shift of the Fermi level by 50 meV. The χ function now looks dramatically different, and is dominated by six peaks at the K points. Since ΓK equals a (3×3) reciprocal lattice vector, this strong peaking at K can lead to a (3×3) response. Detailed calculations show that this peaking at K is already evident, although less pronounced, at a mere $\sim$10 meV shift of the Fermi level. This high sensitivity is a consequence of the proximity of a saddle point near the Fermi level resulting in a low band dispersion along M'-K' (see the bottom panel of Fig. 4). The same low band dispersion is also responsible for the extended Fermi edge discussed above. Thus, the basic mechanism for the phase transition is the same as in traditional Peierls CDW materials, except that defect doping is the source of the instability. As the temperature is lowered, the surface regions affected by the defects grow, and eventually overlap to form a fully developed (3×3) phase below $\sim$100 K [1–4].

In summary, this work clarifies the band structure of Sn/Ge(111) as measured by angle-resolved photoemission. The results are in good agreement with LDA calculations provided the effects of defect and phase mixture are taken into account. Fermi surface nesting does not occur for an ideal surface. However, the response of the system is highly sensitive to charge transfer partly due to the proximity of a saddle point near the Fermi level and the resulting low band dispersion. Doping by defects leads to a strong (3×3) response and a CDW transition that is unconventional in that a mixed phase evolves over a wide temperature range.

The authors thank E. W. Plummer and C. S. Hellberg for helpful discussions. This work was supported by the U.S. Department of Energy (Division of Materials Sciences, Office of Basic Energy Sciences) under Grants No. DEFG02-91ER45439 (T. C. C.) and No. DE-FG02-97ER45632 (M. Y. C.). The Synchrotron Radiation Center of the University of Wisconsin–Madison is supported by the U.S. National Science Foundation under Grant No. DMR-95-31009. An acknowledgment is made to the Donors of the Petroleum Research Fund, administered by the American Chemical Society, and to the U.S. National Science Foundation Grants No. DMR-99-75182 and No. DMR-99-75470 for partial support of the synchrotron beam line operation.

*Email address: t-chiang@uiuc.edu

[1] J. M. Carpinelli, H. H. Weitering, E. W. Plummer, and R. Stumpf, Nature (London) **381**, 398 (1996).
[2] J. M. Carpinelli, H. H. Weitering, M. Bartkowiak, R. Stumpf, and E. W. Plummer, Phys. Rev. Lett. **79**, 2859 (1997).
[3] A. V. Melechko, J. Braun, H. H. Weitering, and E. W. Plummer, Phys. Rev. Lett. **83**, 999 (1999).
[4] A. V. Melechko, J. Braun, H. H. Weitering, and E. W. Plummer, Phys. Rev. B **61**, 2235 (2000); H. H. Weitering, J. M. Carpinelli, A. V. Melechko, J. Zhang, M. Bartkowiak, and E. W. Plummer, Science **285**, 2107 (1999).
[5] *Complex Systems—Science for the 21st Century,* Report of a U.S. Department of Energy, Office of Science Workshop, Berkeley, CA, 1999.
[6] G. Santoro, S. Scandolo, and E. Tosatti, Phys. Rev. B **59**, 1891 (1999).
[7] J. Ortega, R. Pérez, and F. Flores, J. Phys. Condens. Matter **12**, L21 (2000).
[8] G. Le Lay, V. Yu. Aristov, O. Boström, J. M. Layet, M. C. Asensio, J. Avila, Y. Huttel, and A. Cricenti, Appl. Surf. Sci. **123/124**, 440 (1998).
[9] R. I. G. Uhrberg and T. Balasubramanian, Phys. Rev. Lett. **81**, 2108 (1998).
[10] J. Avila, A. Mascaraque, E. G. Michel, M. C. Asensio, G. Le Lay, J. Ortega, R. Pérez, and F. Flores, Phys. Rev. Lett. **82**, 442 (1999).
[11] A. Goldoni and S. Modesti, Phys. Rev. Lett. **79**, 3266 (1997).
[12] O. Bunk, J. H. Zeysing, G. Falkenberg, R. L. Johnson, M. Nielsen, M. M. Nielsen, and R. Feidenhans'l, Phys. Rev. Lett. **83**, 2226 (1999).
[13] T. Kidd, T. Miller, and T.-C. Chiang, Phys. Rev. Lett. **83**, 2789 (1999).